JOURNAL OF GUIDANCE, CONTROL, AND DYNAMICS
Vol. 37, No. 1, January–February 2014

Collinear Three-Craft Coulomb Formation Stability Analysis and Control

Drew R. Jones*
University of Texas at Austin, Austin, Texas 78712
and
Hanspeter Schaub†
University of Colorado, Boulder, Colorado 80309

DOI: 10.2514/1.60293

Coulomb forces associated with charged close-flying satellites can efficiently enable static formation equilibria, in which separation distances remain constant. However, limited Coulomb force controllability presents many challenges in maintaining and maneuvering these inherently unstable formations. This paper studies three-craft collinear equilibria, admitted in the presence of a central body gravity field. Necessary existence conditions for this class of Coulomb formation are given in previous research, and this paper extends these to be sufficient, while using a more accurate Coulomb force model. Stability properties of the resulting configuration cases are analyzed for the first time, and it is shown that each can exhibit marginal stability normal to the orbit plane. Also, it is demonstrated that in-plane perturbations can be asymptotically stabilized, using only craft charging, for the radially aligned configurations. A charge feedback law is derived for this case, and numerical results are provided. These stability and controllability properties correlate with those, previously known, for two- and three-craft (in the absence of gravity) formations. Lastly, invariant manifolds are generated to illustrate dynamic properties of these systems, and the possibility of exploiting the manifold flows to target minimum fuel reconfigurations (shape changes), is discussed.

I. Introduction

SPACECRAFT charge control was considered as early as 1966 by Cover et al. [1], who proposed to use electrostatic forces to inflate and maintain the shape of a large reflecting mesh. The prospect of using this concept in spacecraft (S/C) formation flying is introduced by King et al. [2,3], in which the electric potential (or net charge) of each vehicle is actively controlled, to yield desired intercraft forces. Close-proximity spacecraft have many advantages over a single large craft: overall mass reduction, shape-changing ability, and multi-launch assembly. Free-flying formations have applications in Earth imaging, surveillance, and for enabling separated space-borne interferometry [2,4]. Initially, electric propulsion (EP) systems were proposed for controlling the relative craft motions; however, EP suffers from limited throttle ability and introduces the problem of thruster plume impingement, where thruster ejecta may damage or impede neighboring craft [2]. In contrast, active charge control avoids thruster plumes, has fast throttling (millisecond transitions), and can sustain a given force using less power and fuel than EP [1,2]. Charge control is highly efficient, with specific impulse values as high as 10^{13} s. Active control of a spacecraft charge was successfully executed during the SCATHA [5] and ATS [6] missions, and is currently being used on the CLUSTER [7] mission. Other applications for electrostatic thrusting include advanced docking and rendezvous, autonomous inspection, contactless removal of hazardous material [8], and the deployment/retrieval of instruments [9].

Of particular interest in Coulomb formation flying are constant charge "virtual structures," referred to as static Coulomb formations, in which craft separation distances are in equilibrium. Charge control is demonstrated to be a capable and efficient means for establishing and maintaining geometries that appear frozen, with respect to the Hill frame, a rotating frame with origin at the formation center of mass [2,9]. Milli-Newton levels of forces can be produced over dozens of meters using only watt levels of electrical power. Necessary equilibrium conditions are derived for such formations, analytically for less than five craft (numerically otherwise) and, thus far, all are dynamically unstable [2,9]. It is the three-craft, collinear Hill frame equilibria, in the presence of linearized gravity, that are considered in the current work. This research expands upon the work of Berryman and Schaub [9], by deriving sufficient equilibria conditions and by including the physical effect of plasma shielding. These sufficient conditions yield unique equilibrium regions with varying stability properties, which are explored in detail for the first time. Analogous explicit existence criteria are defined for spinning three-craft collinear equilibria, in the absence of gravitational forces [10,11], and Wang and Schaub expand these to be sufficient for real-valued charges [12]. Stability analyses are carried out for two- and three-craft spinning configurations [13,14], and stable two-body scenarios are identified when the plasma shielding is included [13]. A recent study by Hogan and Schaub demonstrate marginal in-plane stability of particular collinear spinning equilibria, if proper separation distance and speed conditions are met [14].

Unfortunately, Coulomb thrusting has limited reach (from plasma shielding) and controllability and, for example, cannot alter the overall inertial formation angular momentum [15]. Therefore, it is often supplemented with the less-desirable inertial thrust (e.g., EP or chemical), which necessitates hybrid control [16,17]. Methods for maintaining and maneuvering the inherently unstable Coulomb formations remains a challenging and active area of research. Natarajan and Schaub [18] demonstrate that radial two-craft Hill frame equilibria have marginal out-of-plane stability and that charge control alone can asymptotically stabilize in-plane perturbations. Lee et al. [19] go further, developing a Lyapunov stable charge feedback law to maintain two-craft separation distance and rate. In the current research, it is shown that the radial three-craft formation shares these properties, and an in-plane charge feedback law is derived to maintain the formation, substantiated by numerical simulation. Also, relative instability and eigenvector mode properties associated with all of the three-craft collinear configurations are analyzed. In particular,

Presented as Paper 2012-4721 at the AIAA/AAS Astrodynamics Specialists Conference, Minneapolis, MN, 13–16 August 2012; received 11 September 2012; revision received 25 February 2013; accepted for publication 13 April 2013; published online 10 October 2013.

*Graduate Student, Aerospace Engineering and Engineering Mechanics Department, WRW Laboratories. Student Member AIAA.

†Associate Professor, H. Joseph Smead Fellow, Department of Aerospace Engineering Sciences. Senior Member AIAA.

marginal stabilities along particular Hill axes are indicated in the interest of using these facets to reduce station-keeping control effort. Marginal axis stability is exploited during controller design for the two-craft orbit-normal configuration [16] and three-craft spinning equilibria [10,12,20,21]. In addition, feedback control is derived by Inampudi for circular restricted three-body problem equilibrium configurations about Earth–moon libration points [17], and nonlinear controllers are considered and tested for three-craft spinning equilibria [10,20,21].

Another advantageous property of free-flying formations is that they can change shape and therefore be reconfigured as necessary for a particular mission. Methods for realizing the shape-changing ability of Coulomb formations are just being explored, and doing so optimally is very new. Natarajan [22] presents a hybrid (Coulomb and inertial) feedback control to transfer between two-craft Hill frame configurations, and Inampudi adds optimization to those transfers: minimizing time, fuel, or total power usage [17]. Jones and Schaub outline a generalized procedure for targeting minimal ΔV transfers between Coulomb equilibria, in which a parameter optimization formulation is used to differentially correct an uncontrolled and discontinuous initial trajectory along invariant manifolds [23,24]. This method seeks natural flows along manifolds that nearly "hop" from unstable to stable branches, to partially achieve the reconfigurations and thereby reduce ΔV. This is analogous to work in which manifolds are used to design low-thrust transfers in multibody gravity fields, for example, in the work of Russell and Lam [25]. In this paper, the invariant manifold theory is applied to the three-craft collinear equilibria for the first time. The intention is to understand how the method of Jones and Schaub [23,24] may be used and extended to achieve minimal ΔV shape changes for this class of three-craft Coulomb formation.

II. Background and General Model

A. Spacecraft Charge Control Background

A conductive craft surface will naturally exchange ions and electrons with the plasma of space and, as a result, will assume a nonzero electric potential ϕ (measured in volts). When immersed in a plasma, the ideal vacuum potential is effectively limited (or shielded) due to interactions with free particles and photons. The debye length λ_d approximates this shielding, such that a charged particle at a distance $r > \lambda_d$ is unaffected by ϕ. Debye length is a measure of the time-dependent local plasma temperature and density, and experimental data are available in various regimes. For nominal conditions, λ_d is on the order of 0.01 m at low Earth orbit, 200 m at geostationary, and 10 m in the interplanetary regime [26,27]. However, the effective debye length can be many times greater when ϕ is much greater than the plasma energy [26,27], and in GEO, λ_d can be larger for substantial periods of time [28].

A steady state ϕ occurs when the net current to the craft surface is zero [2], and altering ϕ artificially has substantial mission heritage [5–7]. This involves using an electron gun or similar device to eject electrons/ions into the surrounding plasma with sufficient kinetic energy to escape the "potential well." Therefore, the device must have sufficient power to supply a voltage equal to the desired ϕ, at a current at least greater than the incoming environmental current (because this will tend to drive ϕ back to natural equilibrium). In this work, perfectly spherical spacecraft (radius R_{sc}) are assumed and formations near GEO are considered. Each craft's net surface charge q is considered as a control, by allowing q to be analytically related to the truly measurable/controllable parameter ϕ, via Eq. (1), where k_c is the Coulomb constant:

$$\phi = k_c \frac{q}{R_{sc}} \tag{1}$$

Equation (1) holds in a vacuum so long as all spacecraft are assumed to have perfectly conductive outer surfaces of uniform charge density. Additionally, it is accurate in the plasma so long as $R_{sc} \ll \lambda_d$, and as long as the capacitance of any one craft is unaffected by the others. The former is generally true in the presumed GEO altitude, and the latter is a good assumption so long as the craft are sufficiently far apart ($>10R_{sc}$) [22,27]. Such separation distances are enforced throughout this work, in addition to the assumption of a constant and nominal λ_d.

B. Dynamic Model

Formation dynamics are modeled relative to the Hill frame, which is centered at and rotates with a nominal center of mass (c.m.) orbit (assumed circular with semimajor axis a_0 near GEO), as shown in Fig. 1. The Hill frame axes are labeled $\hat{e}_R$ for radial, $\hat{e}_T$ for transverse, and $\hat{e}_N$ for normal. The vehicles then appear statically fixed with respect to the rotating Hill frame for equilibrium configurations admitted by this model. The Hill frame introduces a c.m. constraint given by Eq. (2), where $\mathbf{r}_i$ denotes the position vector relative to the c.m., of craft i (with mass m_i and net charge q_i). In addition to the linearized Clohessy–Wiltshire–Hill equations of relative motion [29], a net Coulomb acceleration defined using the Debye–Hückel point charge model [30] is assumed. The acceleration of craft i is then defined by Eq. (3), where ω is the rotational rate of the reference (c.m.) orbit; $r_{ij} = \|\mathbf{r}_i - \mathbf{r}_j\|$ is the separation distance between crafts i and j; and x, y, and z denote components along the axes $\hat{e}_R$, $\hat{e}_T$, and $\hat{e}_N$, respectively:

$$\sum_i m_i \mathbf{r}_i = 0 \qquad \mathbf{r}_i = [x_i y_i z_i]^T \tag{2}$$

$$\ddot{\mathbf{r}}_i = \begin{bmatrix} 2\omega\dot{y}_i + 3\omega^2 x_i \\ -2\omega\dot{x}_i \\ -\omega^2 z_i \end{bmatrix} + \frac{k_c q_i}{m_i} \left[\sum_{j \neq i}^{j} \frac{q_j (1 + \frac{r_{ij}}{\lambda_d})}{r_{ij}^3 \exp[r_{ij}/\lambda_d]} \mathbf{r}_{ij} \right] \tag{3}$$

The approximate electrostatic model provides a conservative account of the plasma shielding and is demonstrated to be highly accurate in GEO, both experimentally and numerically, for $r_{ij} > 10R_{sc}$ [22,27]. The Lorentz force, which arises as an interaction between an orbiting charged body and Earth's magnetic field, is many orders of magnitude smaller (at GEO) than the Coulomb forces being considered in this paper [31]. Therefore, those effects, although important to other related studies, are ignored. Lastly, the charge products $Q_{ij} = q_i q_j$ are considered here to be fully controllable parameters.

C. Linear Systems and Invariant Manifold Theory Overview

Any equations of formation motion may be written as a first-order ordinary differential equation (ODE) system defined by Eq. (4a), where t is time, $\mathbf{X}$ is the state vector, and $\mathbf{u}$ contains the independent controls. This system can be linearized about some reference state $\mathbf{X}^*$, as shown in Eq. (4b), in which small state perturbations $\delta\mathbf{X}$ from $\mathbf{X}^*$ satisfy a linear ODE system with Jacobian matrix $\mathbf{A}$:

$$\dot{\mathbf{X}} = \mathbf{F}(\mathbf{X}, \mathbf{u}, t) \tag{4a}$$

$$\delta\dot{\mathbf{X}} = \left(\frac{\partial \mathbf{F}}{\partial \mathbf{X}}\right)\Big|_{\mathbf{X}^*} \delta\mathbf{X} = \mathbf{A}\delta\mathbf{X} \tag{4b}$$

The matrix $\mathbf{A}$ can be transformed to Jordan canonical form and decomposed into unstable, stable, and center eigenspaces (E^u, E^s, E^c

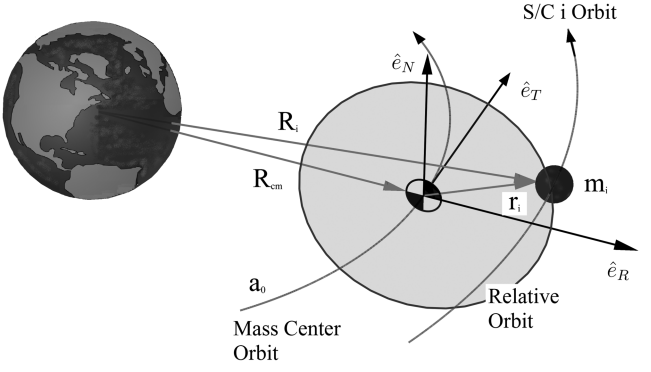

Fig. 1 Rotating Hill frame showing relative position vector $\mathbf{r}_i$.

with dimensions N_u, N_s, and N_c, respectively) [32]. Moreover, the global stable and unstable manifolds (if they exist) are subspaces containing all trajectories (or flows) governed by the original nonlinear system dynamics $\mathbf{F}$, and have the following properties [32]:

1) Unstable manifold W^u is the set of all trajectories that approach $\mathbf{X}^*$ exponentially as $t \to -\infty$, for $t < 0$.

2) Stable manifold W^s is the set of all trajectories that approach $\mathbf{X}^*$ exponentially as $t \to \infty$, for $t > 0$.

3) The manifolds are invariant, and therefore a state contained within W^u or W^s remains in that subspace for all time (e.g., $W^u \leftrightarrow W^s$ flows cannot occur).

4) W^u is tangent to $\pm E^u$ (W^s is tangent to $\pm E^s$) at $\mathbf{X}^*$, with $+E^u$ and $-E^u$ ($+E^s$ and $-E^s$) yielding two branches for W^u (W^s). Also, the manifold subspaces have dimensionality one greater than their corresponding eigenspaces (i.e., W^u has a dimension of $N_u + 1$).

The manifolds can be generated by initiating small maneuvers ($\Delta\mathbf{v}^{u/s} = \pm\epsilon E_{\mathbf{v}}^{u/s}$), where $E_{\mathbf{v}}^{u/s}$ indicates the velocity components of the normalized eigenvectors that span either E^u or E^s, and ϵ is a small number. When constructing W^u, the perturbed states $\mathbf{X}^{\mathbf{u}} = \mathbf{X}^* \pm \epsilon E_{\mathbf{v}}^u$ are propagated forward in time using $\mathbf{F}$; whereas, for W^s, the corresponding perturbed states are propagated backward in time.

III. Three-Craft Collinear Coulomb Formation Existence

Berryman and Schaub [9] show that three-craft collinear equilibrium only exist when the vehicles are aligned along a Hill axis, and they present necessary equilibria conditions, but without including plasma shielding. The equilibria conditions do not ensure real-valued charges (potentials), but a set of real equilibrium charges are known to exist for all Hill axes and separation distances [9]. In this work, necessary and sufficient conditions are derived, with the inclusion of shielding, for the first time. The sufficient conditions establish bounds on the charge products that ensure nonimaginary values, and these bounds present discrete equilibria regions or cases. The stability properties of each of these regions are analyzed here, also for the first time.

Because each craft is located on a single Hill axis, a concise notation is adopted to describe these equilibria, where r_i denotes the craft i signed distance along that line, and d_i denotes the radial magnitude ($d_i = |r_i|$) [9]. Because the craft numbering is arbitrary, it is assumed that $r_1 < 0$ and $r_3 > 0$, as illustrated in Fig. 2, where $d_{ij} = |r_{ij}| = |r_i - r_j|$. The three scalar expressions of Eq. (5) define the three-craft collinear equilibria using this notation, where the term a_d is used to differentiate between the linearized gravitational terms of radial ($a_d = -3$), along-track ($a_d = 0$), and orbit-normal ($a_d = 1$) aligned formations.

$$a_d m_i r_i = \sum_{\substack{j \\ j \neq i}} \left(\frac{\tilde{Q}_{ij}(1 + \frac{d_{ij}}{\lambda_d})[r_i - r_j]}{d_{ij}^3 \exp[d_{ij}/\lambda_d]} \right) \qquad i, j = 1, 2, 3 \tag{5}$$

Equation (5) is derived from Eq. (3), with all time derivatives equal to zero, and with the substitution of scaled charge products $\tilde{Q}_{ij}$, defined in Eq. (6):

$$\tilde{Q}_{ij} = \frac{k_c Q_{ij}}{\omega^2} \tag{6}$$

Two of the three Eq. (5) expressions are linearly dependent. With the inclusion of the Eq. (2) c.m. constraint, a total of three conditions remain, and there are six unknowns: $\tilde{Q}_{12}$, $\tilde{Q}_{13}$, $\tilde{Q}_{23}$, d_1, r_2, and d_3. This underdetermined system is handled by specifying $\tilde{Q}_{13}$, d_1, and d_3 [r_2 found explicitly from Eq. (2)] and then solving $\tilde{Q}_{12}$ and $\tilde{Q}_{23}$ from the Eq. (5) conditions [9]. In addition, in this paper, bounds on $\tilde{Q}_{13}$ are derived, which are sufficient to ensure the individual q_i are nonimaginary.

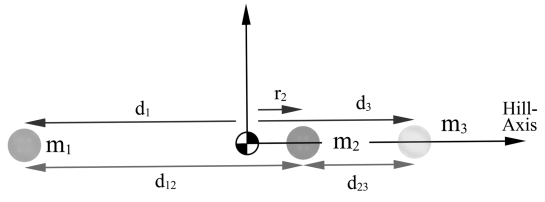

Fig. 2 Three-craft collinear equilibrium geometry and notation.

A. Necessary Equilibrium Conditions with Shielding

Enforcing the assumed sign convention shown in Fig. 2, on the r_i and r_{ij} terms of Eq. (5) and then solving $\tilde{Q}_{12}$ and $\tilde{Q}_{23}$, results in Eqs. (7a) and (7b). These are necessary conditions for three-craft collinear static equilibria, where the θ_{ij} terms account for shielding:

$$\begin{aligned} \tilde{Q}_{12} &= \frac{1}{\theta_{12}}[a_d d_1 m_1 - \theta_{13}\tilde{Q}_{13}] \\ \tilde{Q}_{23} &= \frac{1}{\theta_{32}}[a_d d_3 m_3 - \theta_{13}\tilde{Q}_{13}] \end{aligned} \tag{7a}$$

$$\theta_{ij} = \frac{[1 + d_{ij}/\lambda_d]}{d_{ij}^2 \exp[d_{ij}/\lambda_d]} \tag{7b}$$

Also, scaled individual craft charges $\tilde{q}_i$ are computed, using the Eq. (8) convention:

$$\tilde{q}_1 = \sqrt{\frac{\tilde{Q}_{12}\tilde{Q}_{13}}{\tilde{Q}_{23}}} \qquad \tilde{q}_2 = \frac{\tilde{Q}_{12}}{\tilde{q}_1} \qquad \tilde{q}_3 = \frac{\tilde{Q}_{13}}{\tilde{q}_1} \tag{8}$$

The choice of having $\tilde{q}_1$ positive is not unique, and the signs of charges in Eq. (8) could be reversed if desired.

B. Sufficient Conditions for Real Equilibrium with Shielding

An examination of Eqs. (7a) and (7b) for varying d_3, d_1, and $\tilde{Q}_{13}$ enables sufficient equilibria conditions (bounds on $\tilde{Q}_{13}$) to be defined. These yield regions in the design space, outside of which equilibria cannot exist, and are presented on a case-by-case basis.

1) Along track: $\tilde{Q}_{13} \geq 0$

2) Orbit normal
   a) Case A: $\tilde{Q}_{13} \geq 0$, $\tilde{Q}_{13} \leq m_1 d_1/\theta_{13}$, and $\tilde{Q}_{13} \leq m_3 d_3/\theta_{13}$.
   b) Case B: $\tilde{Q}_{13} > 0$, $\tilde{Q}_{13} \geq m_1 d_1/\theta_{13}$, and $\tilde{Q}_{13} \geq m_3 d_3/\theta_{13}$.

3) Radial
   Case A: $\tilde{Q}_{13} \geq 0$.
   Case B: $\tilde{Q}_{13} < 0$, $|\tilde{Q}_{13}| \leq 3m_1 d_1/\theta_{13}$, and $|\tilde{Q}_{13}| \geq 3m_3 d_3/\theta_{13}$ ($m_1 d_1 \geq m_3 d_3$).
   Case C: $\tilde{Q}_{13} < 0$, $|\tilde{Q}_{13}| \geq 3m_1 d_1/\theta_{13}$, and $|\tilde{Q}_{13}| \leq 3m_3 d_3/\theta_{13}$ ($m_1 d_1 \leq m_3 d_3$).

The free charge product Q_{13} is thus bounded either from above or below (or both above and below for radial cases B and C). Also the sign of $\tilde{Q}_{13}$ explicitly governs the sign for all charge products, and therefore each of the three forces is repulsive or attractive on the basis of these cases. For example, radial case B invokes an attractive force between crafts 1 and 2 and a repulsive force between crafts 2 and 3, whereas radial case C invokes opposite signs on those forces, all due to the relative position and mass of crafts 1 and 3. Furthermore, trivial cases admitted by Eq. (7a), where $\tilde{Q}_{12} = \tilde{Q}_{23} = q_2 = 0$ ($r_2 = 0$), are included in this categorization. These are defined by Eq. (9) and are considered trivial because they simply reduce to the two-craft Hill frame configurations (along each axis):

$$\tilde{Q}_{13} = \frac{a_d m_1 d_1}{\theta_{13}} = \frac{a_d m_3 d_3}{\theta_{13}} \qquad d_1 = \frac{m_3 d_3}{m_1} \tag{9}$$

The only technical difference from the two-craft cases is the addition of a noninteracting craft (craft 2), which is located at the c.m. (origin). The two-craft equilibria and their respective stability properties are examined in detail by various authors [17,18,23].

C. Computing Optimal Charges for a Given Configuration

Because an infinite number of individual charges can produce the equilibria cases described in Sec. III.B, computing ideal or optimal values is of interest. The L_∞ norm of the three q_i is a sensible performance measure to use because that minimizes the largest potential ϕ on any craft. Because ϕ is proportional to the power required (via Ohm's law), a minimum L_∞ measure ensures the entire system can use a charge control device with the lowest possible power requirement. In contrast, an L_1 or L_2 norm would result in a larger (or equal) maximum ϕ, and therefore an individual craft would require more power. The remaining vehicles would then have to accommodate this higher power, with the practical assumption that identical control hardware is used on each.

Determining a specified equilibrium configuration, with minimum L_∞ norm of the charges, is formulated as a constrained nonlinear programming problem, for which many numerical algorithms are available. The cost function to be minimized is $\|\mathbf{q}\|_\infty = \max(|q_1|, |q_2|, |q_3|)$. To handle this function numerically, a new (dummy) variable α is added, along with the constraints $\alpha \geq |q_i|, \forall\ i$. Equations (10a) and (10b) specify the nonlinear program, where $\mathbf{X_p}$ denotes the vector of decision variables:

$$\text{minimize } J(\mathbf{X_p}) = \alpha \qquad \mathbf{X_p} = [\,q_1 \quad q_2 \quad q_3 \quad \alpha\,]^T \tag{10a}$$

$$\text{subject to } \mathbf{C}_{\text{eq}}(\mathbf{X_p}) = 0 \qquad \mathbf{C}(\mathbf{X_p}) \leq 0 \tag{10b}$$

The equality constraints correspond to Eqs. (7a) and (7b), and the inequality constraints correspond to the case-specific sufficient conditions described in Sec. III.B, and also,

$$|q_i| - \alpha \leq 0 \qquad i = 1, 2, 3$$

Moreover, the Sec. III.A necessary and Sec. III.B sufficient conditions provide for the determination of a feasible $\mathbf{X_p}$ initial guess. Numerically, this optimization problem is well behaved and easily solved. Some optimal results, obtained using MATLAB's *fmincon* as the numerical solver, are presented in Table 1, where the power is computed using Ohm's law with a potential (in volts) calculated by substituting $|q_i|_{\max}$ into Eq. (1). An operating current is assumed that is sufficient to overcome the incoming plasma current, during nominal λ_d conditions in GEO ($\approx$80 μA) [2,26,33]. The Table 1 results show that, with optimal charge selection, formations of $|d_1 - d_3| \leq 100$ m can be produced with <10 W of power. Furthermore, these power requirements should be considered high estimates because of the use of a conservative plasma-shielding model, relatively small λ_d, and large current. The radial and orbit-normal configurations exhibit nearly equal power requirements for similar $|d_1 - d_3|$, and the power increases in proportion to $|d_1 - d_3|$. Lastly, along-track results are omitted because it is clear from Eqs. (7a) and (7b) that the optimum occurs when all charges are zero (trivial case).

IV. Three-Craft Collinear Equilibrium Linear Stability Analysis

The equilibrium regions presented in Sec. III.B each have distinct eigenspaces, but all are dynamically unstable. The relative instability and eigenvector modal properties are especially important in the design of feedback stabilization. In this section, a numerical stability analysis demonstrates by example how the eigenspaces (and associated manifold structures) can change as a function of the d_{ij} and alignment axis. As an illustrative example and not an algebraic proof, specific parameter values are used (e.g., a_0, λ_d, and m_i).

Table 1 Minimum charge selection results for three-craft collinear cases

Axis	Case	$\mathbf{d}_1$, m	$\mathbf{d}_3$, m	$\lvert\mathbf{q}_i\rvert_{\max}$, μC	Power, w
Orbit normal	A	30	25	1.72	1.24
Orbit normal	A	40	60	12.29	8.83
Orbit normal	B	30	25	3.52	2.54
Orbit normal	B	40	60	8.27	5.95
Radial	A	30	25	3.33	2.39
Radial	A	40	60	10.59	7.61
Radial	B	30	25	5.32	3.82
Radial	B	30	18	4.64	3.34
Radial	C	40	60	13.34	9.60

In deriving the linearized ODE system as in Eq. (4b), craft 2 is removed via the c.m. condition, reducing the system dimension from 18 to 12. The eigenspaces and invariant manifolds are numerically computed using the Eq. (3) dynamics with $\lambda_d = 180$ m, equal mass craft $m_1 = m_2 = m_3 = m = 150$ kg, and $a_0 = 4.227e^7$ m. For along-track and radial case A configurations, $\tilde{Q}_{13} = 1.0e^4$ is used, whereas $\tilde{Q}_{13}$ is chosen to be just inside the feasible boundary for orbit-normal cases, and $\tilde{Q}_{13}$ is selected equal to the mean of the upper/lower bounds for radial cases B and C. The resulting eigenspace properties, for all cases, are as follows.

1) Along-track: $N_u = N_s = 1$ (distinct real); mode is contained in the $\hat{e}_R - \hat{e}_T$ plane. Perturbations along $\hat{e}_N$ only are marginally stable.

2) Orbit-normal case A: $N_u = N_s = 4$ (two complex pairs); all unstable/stable modes are contained in the $\hat{e}_R - \hat{e}_T$ plane, and therefore perturbations along $\hat{e}_N$ only are marginally stable.

3) Orbit-normal case B: $N_u = N_s = 3$ (one complex pair, one mode real); complex mode in the $\hat{e}_R - \hat{e}_T$ plane.

   a) Small $|d_1 - d_3|$. Real mode is contained in the $\hat{e}_R - \hat{e}_T$ plane. Perturbations along $\hat{e}_N$ only are marginally stable.

   b) Large $|d_1 - d_3|$. Real mode is along $\hat{e}_N$, making $\hat{e}_N$ only perturbations unstable.

4) Radial case A: $N_u = N_s = 2$ (two distinct real); both modes are contained in the $\hat{e}_R - \hat{e}_T$ plane, and perturbations along $\hat{e}_N$ only are marginally stable.

5) Radial cases B and C:

   a) Small $|d_1 - d_3|$. $N_u = N_s = 3$ (one complex pair, one real); all modes are contained in the $\hat{e}_R - \hat{e}_T$ plane. Perturbations along $\hat{e}_N$ only are marginally stable.

   b) Large $|d_1 - d_3|$. $N_u = N_s = 3$ (three distinct real); two modes are contained in the $\hat{e}_R - \hat{e}_T$ plane, and the other mode is entirely along $\hat{e}_N$. Perturbations along $\hat{e}_N$ only are unstable.

In this analysis, there are no stability bifurcations (changes to N_u or N_s) within each case, as a function of d_1, d_3, and $\tilde{Q}_{13}$. Moreover, no bifurcations occur as $\lambda_d \to \infty$ (no shielding) for all cases except for the along-track case, which bifurcates to $N_u = N_s = 0$ (all distinct eigenvalues). What is particularly interesting in this analysis is the differing out-of-orbit plane $\hat{e}_N$ stability for the orbit-normal case B and radial cases B and C, as a function of $|d_1 - d_3|$. This observation is especially important because it demonstrates that marginal out-of-plane stability for the radial configuration (and along-line marginal stability for the orbit-normal case) can be achieved through careful selection of the distances d_1 and d_3 and the charge product $\tilde{Q}_{13}$. Marginal stability along the line-of-sight vector for orbit-normal configurations is shared by the two-craft equilibrium, and this property is used by Natarajan and Schaub [16] to reduce station-keeping control effort for that case. For either axis of alignment, the $\hat{e}_N$ instabilities arise when two craft are in close proximity and have a repulsive Coulomb force that becomes larger than the restorative differential gravity force. Therefore, this instability depends on $|d_1 - d_3|$ as well as $\tilde{Q}_{ij}$ magnitudes, and its existence and the conditions under which it can arise were previously unknown. Jones and Schaub provide a more detailed analysis and explanation concerning this modal bifurcation [34].

V. Invariant Manifolds for the Three-Craft Collinear Equilibria

Invariant manifolds are analyzed to illustrate some of the previously presented stability properties, but also to understand how natural motions may be best exploited to aid in reconfiguring the formations. Reconfigurations of interest include expansions and contractions of the overall distance d_{13}, transfers between equilibrium regions, and transfers between one axis of alignment to another. Moreover, the manifolds could be used to expel or add a craft by transferring between a two- and three-craft equilibrium (with one

craft leaving or entering the system). The linearized ODE systems and assumptions of Sec. IV are used in all numerically generated invariant manifolds that follow. The manifolds are initiated with a $\Delta\mathbf{v}$ perturbation (for each craft) along the associated eigenspace vectors, with $\epsilon = 0.1$ mm/s.

A. Manifold Structures

It is known that all orbit-normal and radial cases B and C (for $|d_1 - d_3|$ large) unstable/stable manifolds are in $\Re^6$, whereas the remaining cases are in $\Re^4$, because modal motion is confined to the $\hat{e}_R - \hat{e}_T$ plane. Radial case A unstable manifolds are illustrated in Fig. 3a, which shows that motion is confined to the reference orbit plane. There is strong attractive Coulomb interaction between two of the inner craft on each branch, which makes the trajectories have many intersections. Figure 3b demonstrates the out-of-plane instability for case B, resulting in an $\Re^3$ (in position) manifold structure. On one branch, the attractive forces bring all vehicles together, which, in turn, increases the repulsive force on craft 2, thereby giving it an increasing z component. On the other branch, the repulsive force on craft 2 causes it to move away from the other two craft. For both branches, the purely real $\hat{e}_N$ unstable mode is quite distinct.

Along-track stable and unstable manifolds are illustrated in Figs. 4a and 4b. There is great symmetry between stable and unstable branches, and it is rather intuitive to visualize a transfer trajectory from unstable to stable manifolds, which could expand or contract this formation with little control effort. Finally, some orbit-normal unstable manifolds are illustrated in Figs. 5a and 5b. The case A manifolds resemble the two-craft orbit-normal manifolds, which also exhibit along-line marginal stability. The case B manifolds have strong Coulomb interaction between crafts 2 and 3 because of their attractive force. It is this attraction that can cause the $\hat{e}_N$ unstable mode for that case.

B. Reconfigurations Between Three-Craft Collinear Equilibria Along Manifolds

The motivation here is to identify reconfiguration scenarios, in which natural manifold flows can nearly provide the transfer, and also situations in which such an approach becomes impractical. The identification and improved quality of these initial guess (IG) trajectories, represent important prerequisite steps to extending the previously developed method for converging fuel optimal reconfigurations [23,24] to three-craft collinear formations. As mentioned previously, expansions and contractions between along-track configurations are relatively intuitive to visualize. Figure 6 demonstrates an example IG trajectory, which would expand the along-track configuration, increasing d_{13} by 10 m and also moving r_2 from $+5$ to $+3$ m. This is an IG only, because there are state

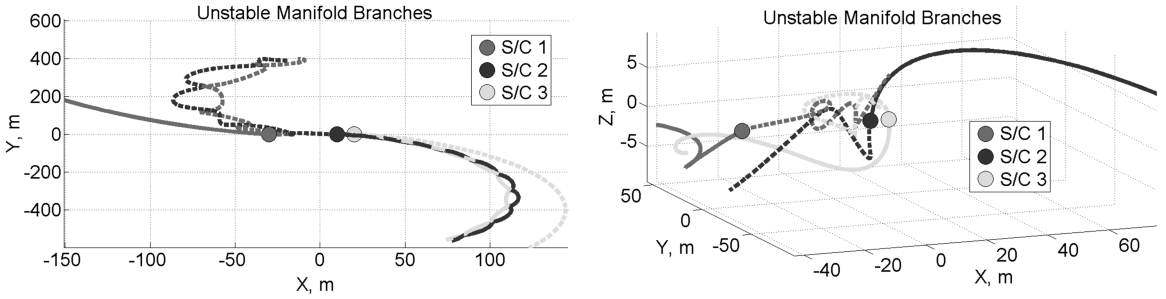

a) Case A: 1.0 T_p, d_3 = 25 m, and $\tilde{Q}_{13} = 1.0e^4$ b) Case B: 0.5 T_p, d_3 = 18 m, and $\tilde{Q}_{13} = -2.56e^7$

Fig. 3 Three-craft radial unstable manifolds for $d_1 = 30$ m.

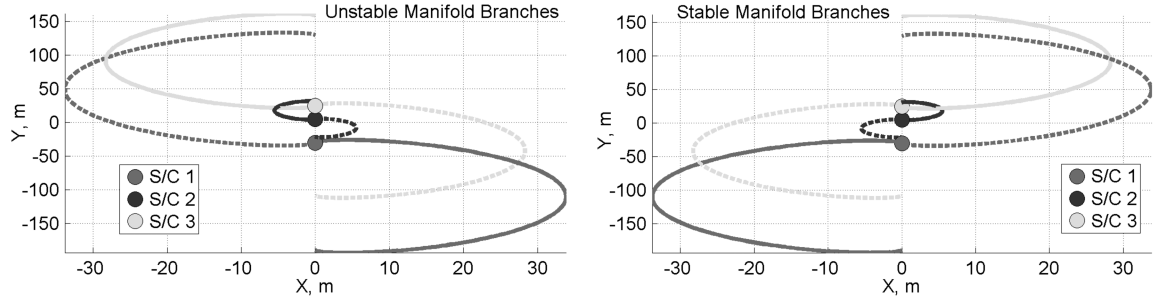

a) Unstable b) Stable

Fig. 4 Three-craft along-track invariant manifolds for $1.0T_p$, $d_1 = 30$ m, $d_3 = 25$ m, and $\tilde{Q}_{13} = 1.0e^4$.

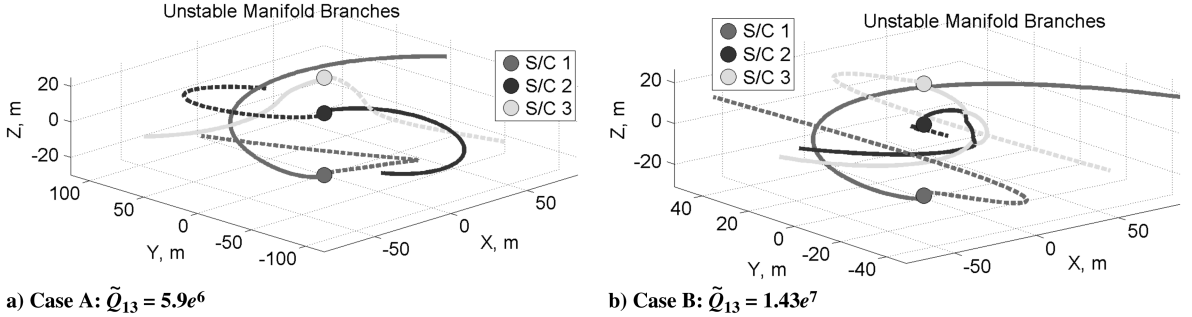

a) Case A: $\tilde{Q}_{13} = 5.9e^6$ b) Case B: $\tilde{Q}_{13} = 1.43e^7$

Fig. 5 Three-craft orbit-normal unstable manifolds for $1.0T_p$, $d_1 = 30$ m, and $d_3 = 25$ m.

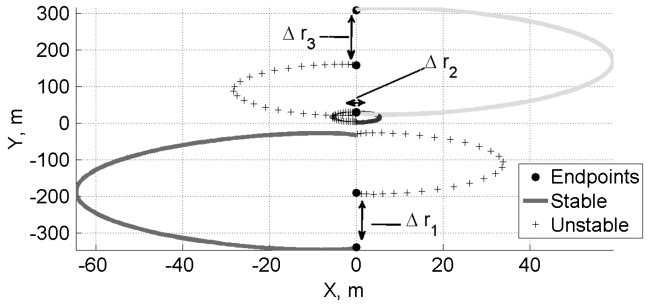

Fig. 6 Along-track initial guess expansion trajectory along manifolds propagated $1T_p$: $d_1 = 30 \rightarrow 36$ m and $d_3 = 25 \rightarrow 34$ m.

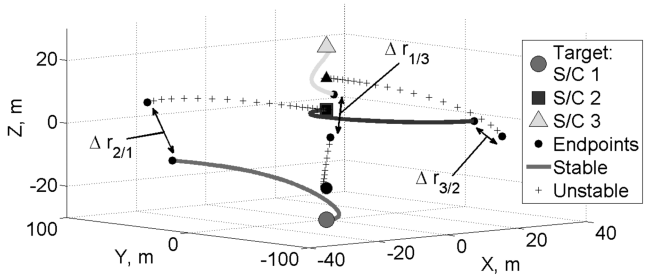

Fig. 7 Orbit-normal initial guess expansion trajectory along manifolds propagated $0.7T_p$: $d_1 = 20 \rightarrow 30$ m and $d_3 = 15 \rightarrow 25$ m.

discontinuities between unstable and stable manifolds at the patch point (endpoints of near manifold intersection on the plot). Nevertheless, it is likely that these discontinuities could be differentially corrected to yield a continuous transfer with little control effort, as demonstrated by Jones and Schaub [23,24] for two-craft Hill frame equilibria, where ΔV is minimized.

Another IG expansion example is illustrated in Fig. 7 for the orbit-normal case A configuration and for an increased d_{13} of 20 m (r_2 constant). This transfer is more difficult to visualize because it is $\Re^3$ (in position) and because the velocity directions are hard to ascertain. In addition, for expansions of this configuration, the manifolds are best exploited when the spacecraft numbering changes. Therefore, in Fig. 7, craft 1 moves to the d_3 slot, craft 2 to d_1, and craft 3 to r_2. This is completely reasonable, assuming equal mass craft and because the charges can be transitioned extremely fast (nearly impulsive).

The radial configuration manifolds are not as readily useful to aid in contraction and expansion transfers. Fortunately, these configurations turn out to be fully controllable in the $\hat{e}_R - \hat{e}_T$ plane using only charge control, as demonstrated in Sec. VI. This means that charge control alone can be used to maintain, expand, and contract these cases, and therefore using manifolds to reduce inertial thrust cost is unnecessary.

VI. Three-Craft Collinear Formation Orbit Plane Feedback Stabilization

The along-track and radial configurations have unstable/stable manifolds contained in the $\hat{e}_R - \hat{e}_T$ plane (reference orbit plane) and are considered here. These exhibit marginal out-of-orbit plane stability, and therefore a reduced system controller is designed considering only planar $\hat{e}_R - \hat{e}_T$ dynamics. It is assumed that all craft are of equal mass ($m = 150$ kg) and, initially, plasma shielding is assumed negligible ($\lambda_d \rightarrow \infty$). Scaled charge products $\tilde{Q}_{ij}$, defined by Eq. (6), are then substituted into the $\ddot{\mathbf{r}}_1$ and $\ddot{\mathbf{r}}_3$ Eq. (3) expressions, after $\mathbf{r}_2$ variables are explicitly removed via the Eq. (2) c.m. constraint. The resulting $\hat{e}_R - \hat{e}_T$ terms, given by Eqs. (11a) and (11b), represent scaled craft 1 and 3 accelerations:

$$\mathbf{r}_1'' = \frac{\ddot{\mathbf{r}}_1}{\omega^2} = \begin{bmatrix} 2\dot{y}_1/\omega + 3x_1 \\ -2\dot{x}_1/\omega \end{bmatrix} + \frac{\tilde{Q}_{13}}{md_{13}^3}\begin{bmatrix} x_1 - x_3 \\ y_1 - y_3 \end{bmatrix} + \frac{\tilde{Q}_{12}}{md_{12}^3}\begin{bmatrix} 2x_1 + x_3 \\ 2y_1 + y_3 \end{bmatrix} \tag{11a}$$

$$\mathbf{r}_3'' = \frac{\ddot{\mathbf{r}}_3}{\omega^2} = \begin{bmatrix} 2\dot{y}_3/\omega + 3x_3 \\ -2\dot{x}_3/\omega \end{bmatrix} + \frac{\tilde{Q}_{13}}{md_{13}^3}\begin{bmatrix} x_3 - x_1 \\ y_3 - y_1 \end{bmatrix} + \frac{\tilde{Q}_{23}}{md_{12}^3}\begin{bmatrix} 2x_3 + x_1 \\ 2y_3 + y_1 \end{bmatrix} \tag{11b}$$

where the substitution of the scaled charge products has introduced a time transformation into the equations of motion, as defined by Eq. (12). This transform to the variable τ reduces numerical integration error and helps to prevent poor scaling of the linearized dynamics' matrices:

$$\mathrm{d}\tau = \omega \mathrm{d}t \;\; (\zeta)' = \frac{\mathrm{d}\zeta}{\mathrm{d}\tau} = \frac{1}{\omega}\frac{\mathrm{d}\zeta}{\mathrm{d}t} \tag{12}$$

Next, Eqs. (11a) and (11b) are linearized about the equilibrium state $\mathbf{X}^*$, yielding a time-invariant controlled system, defined in general state-space form by Eq. (13):

$$\delta\mathbf{X}' = \mathbf{A}\delta\mathbf{X} + \mathbf{B}\mathbf{u} \quad \delta\mathbf{X} = \begin{bmatrix} \delta\mathbf{r}_1 \\ \delta\mathbf{r}_3 \\ \delta\mathbf{v}_1 \\ \delta\mathbf{v}_3 \end{bmatrix}_{8\times 1} \quad \mathbf{u} = \begin{bmatrix} \delta q_1 \\ \delta q_2 \\ \delta q_3 \end{bmatrix}_{3\times 1} \tag{13}$$

Matrices $\mathbf{A}$ and $\mathbf{B}$ are given explicitly for the radial configuration in Eqs. (14a) and (14b), where $\tilde{Q}_{ij}^*$ ($\tilde{q}_i^*$), d_{ij}, and r_i denote equilibrium scaled charge products (scaled charges), separation distances, and signed distances, respectively.

$$\mathbf{A} = \begin{bmatrix} 0 & 0 & 0 & 0 & 1 & 0 & 0 & 0 \\ 0 & 0 & 0 & 0 & 0 & 1 & 0 & 0 \\ 0 & 0 & 0 & 0 & 0 & 0 & 1 & 0 \\ 0 & 0 & 0 & 0 & 0 & 0 & 0 & 1 \\ 3 - \frac{4\tilde{Q}_{12}^*}{md_{12}^3} - \frac{2\tilde{Q}_{13}^*}{md_{13}^3} & 0 & -\frac{2\tilde{Q}_{12}^*}{md_{12}^3} + \frac{2\tilde{Q}_{13}^*}{md_{13}^3} & 0 & 0 & 2 & 0 & 0 \\ 0 & \frac{2\tilde{Q}_{12}^*}{md_{12}^3} + \frac{\tilde{Q}_{13}^*}{md_{13}^3} & 0 & \frac{\tilde{Q}_{12}^*}{md_{12}^3} - \frac{\tilde{Q}_{13}^*}{md_{13}^3} & -2 & 0 & 0 & 0 \\ -\frac{2\tilde{Q}_{23}^*}{md_{23}^3} + \frac{2\tilde{Q}_{13}^*}{md_{13}^3} & 0 & 3 - \frac{4\tilde{Q}_{23}^*}{md_{23}^3} - \frac{2\tilde{Q}_{13}^*}{md_{13}^3} & 0 & 0 & 0 & 0 & 2 \\ 0 & \frac{\tilde{Q}_{23}^*}{md_{23}^3} - \frac{\tilde{Q}_{13}^*}{md_{13}^3} & 0 & \frac{2\tilde{Q}_{23}^*}{md_{23}^3} + \frac{\tilde{Q}_{13}^*}{md_{13}^3} & 0 & 0 & -2 & 0 \end{bmatrix} \tag{14a}$$

$$\mathbf{B}=\begin{bmatrix} \mathbf{0}_{4\times1} & \mathbf{0}_{4\times1} & \mathbf{0}_{4\times1} \\ \frac{|\tilde{q}_1^*||\tilde{q}_2^*(2r_1+r_3)}{md_{12}^3}+\frac{|\tilde{q}_1^*||\tilde{q}_3^*(r_1-r_3)}{md_{13}^3} & \frac{|\tilde{q}_2^*||\tilde{q}_1^*(2r_1+r_3)}{md_{12}^3} & \frac{|\tilde{q}_3^*||\tilde{q}_1^*(r_1-r_3)}{md_{13}^3} \\ 0 & 0 & 0 \\ \frac{|\tilde{q}_1^*||\tilde{q}_3^*(r_3-r_1)}{md_{13}^3} & \frac{|\tilde{q}_2^*||\tilde{q}_3^*(2r_3+r_1)}{md_{23}^3} & \frac{|\tilde{q}_3^*||\tilde{q}_2^*(2r_3+r_1)}{md_{23}^3}+\frac{|\tilde{q}_3^*||\tilde{q}_1^*(r_3-r_1)}{md_{13}^3} \\ 0 & 0 & 0 \end{bmatrix} \tag{14b}$$

The $|\tilde{q}_i^*|$ are used to scale the **B** matrix such that it has equal order-of-magnitude terms as those in **A**. This numerical scaling is crucial in successfully computing feedback gains numerically. Also, using the individual charges in **u**, as opposed to charge products, ensures that real-valued q_i are maintained. A charge feedback law is then defined by Eq. (15), where **K** is a full state feedback gain matrix:

$$\begin{bmatrix} \tilde{q}_1(\tau) \\ \tilde{q}_2(\tau) \\ \tilde{q}_3(\tau) \end{bmatrix} = \begin{bmatrix} \tilde{q}_1^* \\ \tilde{q}_2^* \\ \tilde{q}_3^* \end{bmatrix} + \begin{bmatrix} |\tilde{q}_1^*|\delta q_1(\tau) \\ |\tilde{q}_2^*|\delta q_2(\tau) \\ |\tilde{q}_3^*|\delta q_3(\tau) \end{bmatrix}$$

$$\mathbf{u} = \begin{bmatrix} \delta q_1(\tau) \\ \delta q_2(\tau) \\ \delta q_3(\tau) \end{bmatrix} = -\mathbf{K}\delta\mathbf{X}(\tau) \tag{15}$$

The along-track and all radial cases have linearized systems that are fully controllable, made possible because of the coupling between x and y perturbations in the **A** matrix [35]. In contrast, the orbit-normal configurations are not fully controllable in the orbit plane and some inertial thrusting would be required to maintain them. It is demonstrated here, for the first time, that $\hat{e}_R - \hat{e}_T$ planar perturbations can be asymptotically stabilized for the radial configuration, using only charge control (no inertial thrust). An analogous result is demonstrated by Natarajan and Schaub [18] for the radial two-craft configuration. From the state-space model of Eqs. (14a) and (14b), the gain matrix **K** is determined by solving the standard linear quadratic regulator (LQR) problem [35].

A. Radial Feedback Controller Numerical Simulations

For the presented simulations, the LQR weighting matrices **Q** and **R** are both set to identity. The Coulomb configurations are numerically integrated using the nonlinear equations of motion given by Eqs. (11a) and (11b). Also, the values in Secs. IV and V for m, a_0, and Q_{13} are used here for a nominal configuration of $d_1 = 30$ m and $d_3 = 25$ m. Figures 8a and 8b illustrate position perturbation and charge control histories after an initial $\Delta\mathbf{v}$ to crafts 1 and 3, with equal x and y components of 0.01 mm/s. Figures 9a and 9b also show a controlled response, but after initial disturbances in position to all three craft, thereby demonstrating additional robustness in the control. The initial position perturbations for Figs. 9a and 9b are $\Delta x_1 = -0.5$, $\Delta x_2 = 0.18$, $\Delta x_3 = 0.32$, $\Delta y_1 = 0.08$, $\Delta y_2 = -0.056$, and $\Delta y_3 = -0.024$ m. Note that the required nominal charge levels for this radial equilibria are quite small, μC order, despite the fact that minimum L_∞-norm charge selection is not implemented in this simulation. Also, the charge variations required to remove the initial disturbances are relatively small. This controller methodology is easily extended to include shielding, with verifiable asymptotic stabilization. However, numerical simulations and the linearized matrices **A** and **B** with plasma shielding included are omitted for brevity. Lastly, the response characteristics and robustness of this preliminary control design might require refining, specifically by tuning the LQR weighting matrices, and such improvements should consider varying parameter values (e.g., craft masses).

B. Along-Track Feedback Control

Natarajan shows that there exist no real-valued gains that can stabilize the two-craft along-track Coulomb formations, thereby necessitating some inertial thrusting [22]. In contrast, the three-craft along-track configuration does satisfy the linear controllability condition; however, it is very nearly uncontrollable numerically and highly sensitive to perturbations. This assessment of near uncontrollability is made by computing a distance measure from the true system to an uncontrollable state-space system, using the method of Boley and Lu [36]. The measure is small for the along-track case, but relatively large for the radial cases. These difficulties make a charge-only controller impractical, and perhaps even impossible, for

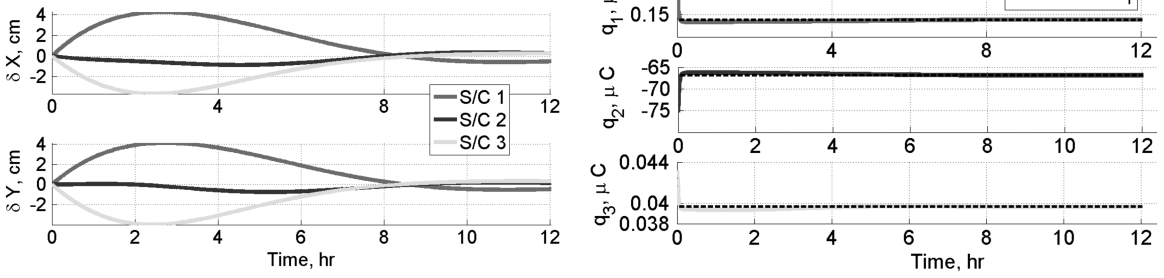

a) Position Perturbations b) Charge History

Fig. 8 Radial case A planar controlled response to initial S/C 1,3 Δv perturbations.

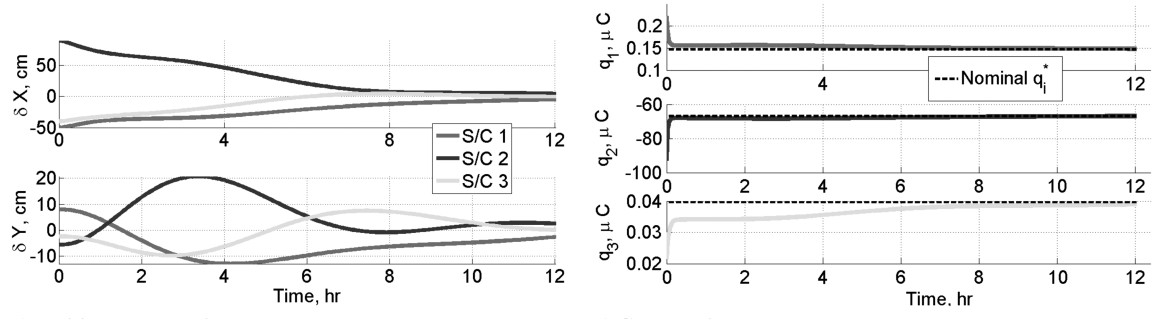

a) Position Perturbations b) Charge History

Fig. 9 Radial case A planar controlled response to initial S/C 1-3 Δr perturbations.

the along-track formation. A coordinate change in the dynamics or the adoption of a nonlinear controller might alleviate some of these difficulties; otherwise, a hybrid control would be necessary to stabilize such a formation.

VII. Conclusions

Necessary and sufficient conditions that enable three-craft collinear static formations are derived in the presence of a linearized gravity model and include partial Coulomb force shielding. A detailed stability analysis for each of the resulting equilibrium is carried out, which demonstrates that marginal stability, normal to the orbit plane, can be achieved, although it is not assured for all cases. Furthermore, numerical simulation illustrates that a linearized charge feedback law (without inertial thrusting) is capable of asymptotically stabilizing in-plane perturbations for the radial configuration. These results were previously unknown and demonstrate how the dynamic properties of these systems may be used to reduce station-keeping control effort. Control laws to stabilize the remaining three-craft collinear configurations are lacking, but this paper presents stability and controllability properties for these cases, which suggest that some inertial thrusting will be required. Further work should focus on these challenges, as well as on improving the robustness of the radial configuration control law, relaxing some of the assumptions used, and possibly incorporating nonlinear control. Lastly, prominent continuous disturbances, such as solar radiation pressure, should be tested to validate the control designs.

Invariant manifold theory is applied to all equilibrium configurations and examples are given that illustrate possible scenarios in which the manifolds may be exploited to reduce the cost associated with reshaping these formations. This analysis suggests that a previously demonstrated methodology for targeting minimal ΔV transfers between two-craft Coulomb equilibria, along manifolds, can be applied to the three-craft configurations as well. Future research will continue to investigate initial trajectories, where unstable manifold flows nearly intersect stable flows and thereby lend themselves to differential correction to match continuity. Such reconfigurations realize the advantageous property of Coulomb formations to change shape using charge control, preferably with as little inertial thrusting as possible.

Acknowledgment

This research was made with government support under and awarded by the Department of Defense through the National Defense Science and Engineering Graduate Fellowship Program.

References

[1] Cover, J. H., Knauer, W., and Maurer, H. A., "Lightweight Reflecting Structures Utilizing Electrostatic Inflation," U.S. Patent 3,546,706, Oct. 1966.

[2] King, L., Parker, C., Deshmukh, S., and Chong, J., "Spacecraft Formation-Flying Using Inter-Vehicle Coulomb Forces," NASA Inst. for Advanced Concepts, Jan. 2002.

[3] King, L., Parker, C., Deshmukh, S., and Chong, J., "Study of Interspacecraft Coulomb Forces and Implications for Formation Flying," *Journal of Propulsion and Power*, Vol. 19, No. 3, 2003, pp. 497–505.
doi: 10.2514/2.6133

[4] Lawson, P., and Dooley, J., "Technology Plan for the Terrestrial Planet Finder Interferometer," NASA Jet Propulsion Lab. TR-05-5, June 2005.

[5] Mullen, E., Gussenhoven, M., and Hardy, D., "SCATHA," *Journal of the Geophysical Sciences*, Vol. 91, No. A2, 1986, pp. 1474–1490.

[6] Whipple, E., and Olsen, R., "Importance of Differential Charging for Controlling Both Natural and Induced Vehicle Potentials on ATS-5 and ATS-6," *Proceedings of the Third Spacecraft Charging Technology Conference*, 1980, pp. 888–893.

[7] Escoubet, C., Fehringer, M., and Goldstein, M., "The Cluster Mission," *Annales Geophysicae*, Vol. 19, Nos. 10/12, 2001, pp. 1197–1200.
doi:10.5194/angeo-19-1197-2001

[8] Moorer, D., and Schaub, H., "Geosynchronous Large Debris Reorbiter: Challenges and Prospects," *AAS/AIAA Kyle T. Alfriend Astrodynamics Symposium*, American Astronautical Society Paper 10-311, May 2010.

[9] Berryman, J., and Schaub, H., "Analytical Charge Analysis for Two- and Three-Craft Coulomb Formations," *Journal of Guidance, Control, and Dynamics*, Vol. 30, No. 6, 2007, pp. 1701–1710.
doi: 10.2514/1.23785

[10] Hussein, I. I., and Schaub, H., "Stability and Control of Relative Equilibria for the Three-Spacecraft Coulomb Tether Problem," *Acta Astronautica*, Vol. 65, Nos. 5–6, 2009, pp. 738–754.
doi: 10.1016/j.actaastro.2009.03.035

[11] Hogan, E., and Schaub, H., "Collinear Invariant Shapes for Three-Craft Coulomb Formations," *AIAA/AAS Astrodynamics Specialists Conference*, AIAA Paper 2010-7954, Aug. 2010.
doi: 10.2514/6.2010-7954.

[12] Wang, S., and Schaub, H., "Nonlinear Charge Control for a Collinear Fixed-Shape Three-Craft Equilibrium," *Journal of Guidance, Control, and Dynamics*, Vol. 34, No. 2, 2011, pp. 359–366.
doi: 10.2514/1.52117

[13] Schaub, H., and Hussein, I. I., "Stability and Reconfiguration Analysis of a Circulary Spinning Two-Craft Coulomb Tether," *IEEE Transactions on Aerospace and Electronic Systems*, Vol. 46, No. 4, 2010, pp. 1675–1686.
doi:10.1109/TAES.2010.5595587

[14] Hogan, E., and Schaub, H., "Linear Stability and Shape Analysis of Spinning Three-Craft Coulomb Formations," *Celestial Mechanics and Dynamical Astronomy*, Vol. 112, No. 2, 2012, pp. 131–148.
doi: 10.1007/s10569-011-9387-6

[15] Schaub, H., and Kim, M., "Differential Orbit Element Constraints for Coulomb Satellite Formations," *AIAA/AAS Astrodynamics Specialists Conference*, AIAA Paper 2004-5213, 2004.

[16] Natarajan, A., and Schaub, H., "Hybrid Control of Orbit-Normal and Along-Track Two-Craft Coulomb Tethers," *AAS/AIAA Space Flight Mechanics Meeting*, American Astronautical Society Paper 07-193, Jan.–Feb. 2007.

[17] Inampudi, R., Two-Craft Coulomb Formation Study About Circular Orbits and Libration Points, Ph.D. Thesis, Univ. of Colorado, Boulder, CO, 2010.

[18] Natarajan, A., and Schaub, H., "Linear Dynamics and Stability Analysis of a Two-Craft Coulomb Tether Formation," *Journal of Guidance, Control, and Dynamics*, Vol. 29, No. 4, 2006, pp. 831–838.
doi: 10.2514/1.16480

[19] Lee, D.-H., Kumar, K., and Bang, H., "Formation Flying of Small Satellites Using Coulomb Forces," *International Journal of Aeronautical and Space Sciences*, Vol. 7, No. 1, 2005, pp. 84–90.
doi: 10.5139/IJASS.2006.7.1.084

[20] Wang, S., and Schaub, H., "One-Dimensional Three-Craft Coulomb Structure Control," *Seventh International Conference on Dynamics and Control of Systems and Structures in Space*, Greenwich, England, June 2006.

[21] Jasch, P., Hogan, E., and Schaub, H., "Stability Analysis and Out-of-Plane Control of Collinear Spinning Three-Craft Coulomb Formations," *AAS/AIAA Spaceflight Mechanics Meeting*, AIAA Paper 2012-151, Jan.–Feb. 2012.

[22] Natarajan, A., A Study of Dynamics and Stability of Two-Craft Coulomb Tether Formations, Ph.D. Thesis, Virginia Polytechnic Inst. and State Univ., Blacksburg, VA, 2007.

[23] Jones, D. R., "Optimal Reconfiguration of Coulomb Formations Along Invariant Manifolds," *AAS/AIAA Spaceflight Mechanics Meeting*, American Astronautical Society Paper 12-104, Jan.–Feb. 2012.

[24] Jones, D. R., and Schaub, H., "Optimal Reconfigurations of Two-Craft Coulomb Formations Along Manifolds," *Acta Astronautica*, Vol. 83, No. 1, Feb.–March 2013, pp. 108–118.
doi:10.1016/j.actaastro.2012.10.028

[25] Russell, R., and Lam, T., "Designing Ephemeris Capture Trajectories at Europa Using Unstable Periodic Orbits," *Journal of Guidance, Control, and Dynamics*, Vol. 30, No. 2, March–April 2007, pp. 482–491.
doi:10.2514/1.22985

[26] Seubert, C., Panosian, S., and Schaub, H., "Attitude and Power Analysis of Two-Node, Multi-Tethered Coulomb Structures," *Journal of Spacecraft and Rockets*, Vol. 48, No. 6, 2011, pp. 1033–1045.
doi: 10.2514/1.52185

[27] Stiles, L., Seubert, C., and Schaub, H., "Effective Coulomb Force Modeling in a Space Environment," *AAS/AIAA Spaceflight Mechanics Meeting*, American Astronautical Society Paper 12-105, Jan.–Feb. 2012.

[28] Denton, M., Thomsen, M., Korth, H., Lynch, S., Zhang, J., and Liemohn, M., "Bulk Plasma Properties at Geosynchronous Orbit," *Journal of Geophysical Research*, Vol. 110, No. A07223, 2005.

[29] Clohessy, W., and Wiltshire, R., "Terminal Guidance System for Satellite Rendezvous," *Journal of the Aerospace Sciences*, Vol. 27, No. 9, 1960, pp. 653–658.
doi: 10.2514/8.8704

[30] Bittencourt, J., *Fundamentals of Plasma Physics*, Springer–Verlag, New York, 2004, Chap. 1.

[31] Saaj, C., Lappas, V., Richie, D., Peck, M., Streetman, B., and Schaub, H., "Electrostatic Forces for Satellite Swarm Navigation and Reconfiguration," ESA TR-ARIADNA-05/4107b, 2006.

[32] Guckenheimer, J., and Holmes, P., *Nonlinear Oscillations, Dynamical Systems, and Bifurcations of Vector Fields*, Springer, New York, 1997, pp. 10–16.

[33] Pettazzi, L., Kruger, H., Theil, S., and Izzo, D., "Electrostatic Forces for Satellite Swarm Navigation and Reconfiguration," ESA TR-ARIADNA-05/4107a, 2006, pp. 13–14, 221–226.

[34] Jones, D. R., and Schaub, H., "Collinear Three-Craft Coulomb Formation Stability Analysis and Control," *AIAA/AAS Astrodynamics Specialists Conference*, AIAA Paper 2012-4721, Aug. 2012.

[35] Tsui, C.-C., *Robust Control System Design: Advanced State Space Techniques*, 2nd ed., Marcel Dekker, New York, 2004.

[36] Boley, D., and Lu, W.-S., "Measuring How Far a Controllable System is from an Uncontrollable One," *IEEE Transactions on Automatic Control*, Vol. 31, No. 3, 1986, pp. 249–251.
doi:10.1109/TAC.1986.1104240